JOURNAL OF PETROLOGY | VOLUME 41 | NUMBER 7 | PAGES 1195–1206 | 2000

Volatile Components, Magmas, and Critical Fluids in Upwelling Mantle

PETER J. WYLLIE[1]* AND IGOR D. RYABCHIKOV[2]

[1]DIVISION OF GEOLOGICAL AND PLANETARY SCIENCES, CALIFORNIA INSTITUTE OF TECHNOLOGY, PASADENA, CA 91125, USA

[2]INSTITUTE FOR GEOLOGY OF ORE DEPOSITS, IGEM, RUSSIAN ACADEMY OF SCIENCES, STAROMONETNY, PEREULOK 35, MOSCOW 109017, RUSSIA

RECEIVED SEPTEMBER 7, 1999; REVISED TYPESCRIPT ACCEPTED JANUARY 14, 2000

*The phase diagram for lherzolite–CO_2–H_2O provides a framework for interpreting the distribution of phase assemblages in the upper mantle with various thermal structures, in different tectonic settings. Experiments show that at depths >80 km, the near-solidus partial melts from lherzolite–CO_2–H_2O are dolomitic, changing through carbonate–silicate liquids with rising temperatures to mafic liquids; vapor, if it coexists, is aqueous. Experimental data from simple systems suggest that a critical end-point (K) occurs on the mantle solidus at an undetermined depth. Isobaric (*T–X*) phase diagrams for volatile-bearing systems with K elucidate the contrasting phase relationships for lherzolite–CO_2–H_2O at depths below and above a critical end-point, arbitrarily placed at 250 km. At levels deeper than K, lherzolite can exist with dolomitic melt, aqueous vapor, or with critical fluids varying continuously between these end-members. Analyses of fluids in microinclusions of fibrous diamonds reveal this same range of compositions, supporting the occurrence of a critical end-point. Other evidence from diamonds indicates that the minimum depth for this end-point is 125 km; maximum depth is not constrained. Constructed cross-sections showing diagrammatically the phase fields intersected by upwelling mantle indicate how rising trace melts may influence trace element concentrations within a mantle plume.*

KEY WORDS: *mantle solidus; critical end-point; dolomitic magma; diamond inclusions; critical fluids*

INTRODUCTION

The dominant volatile components of the Earth's interior, species of C–H–O, may be dissolved in the molten metallic core, and in solid carbides, hydrides and oxides in the deep mantle. There is compelling evidence for the passage of oxidized H_2O and CO_2 vapors through the lithosphere from mantle samples, but the changes occurring in the fluid species of C–H–O between the lower and upper mantle are not determined. Their speciation and distribution can be calculated if assumptions are made for temperatures and oxygen fugacities, both of which may vary in space and time.

The presence of H_2O and CO_2 in the upper mantle has significant consequences for the depths and temperatures of magma formation, rheology, magma compositions, and the distribution of trace elements. From phase relationships in the system lherzolite–CO_2–H_2O we estimate the distribution of aqueous vapors and carbonate-rich liquids in the cylindrical structure of a mantle plume, and explore the consequences if a critical end-point occurs on the solidus. The results imply the existence of fluids continuous between a dolomitic liquid and an aqueous vapor at depths greater than a critical end-point (Ryabchikov & Wyllie, 1991; Wyllie & Ryabchikov, 1992). These compositions correspond closely to the fluids trapped in microinclusions in fibrous diamonds (Schrauder & Navon, 1994). Navon's (1991) estimate of 125–210 km for the minimum trapping depths of the fluid inclusions is consistent with the occurrence of a critical end-point on the mantle solidus phase boundary at a minimum depth of 125 km. This depth estimate is consistent with Ryabchikov's (1988) experimentally based prediction of a critical end-point on the peridotite-H_2O system between 3 and 4 GPa, and with the pressure of 3·25

*Corresponding author. Telephone: +1-626-395-6461. Fax: +1-626-795-6028. e-mail: wyllie@caltech.edu

© Oxford University Press 2000

GPa for a critical end-point determined experimentally by Boettcher & Wyllie (1969*a*) on the solidus of the simpler subsystem $CaO–SiO_2–CO_2–H_2O$.

VOLATILE COMPONENTS IN MANTLE

Bell & Rossman (1992) reported results from the first systematic study of mantle H_2O stored in minerals that are nominally anhydrous, and their calculated H_2O contents range from 25 ppm in spinel lherzolite to 175 ppm in garnet lherzolite. The volatile component concentrations in basalt probably provide the most realistic estimate of average mantle volatile components. Using data for basaltic glasses and mass of water in exosphere, O'Neill & Palme (1998) calculated H_2O contents in depleted and primitive mantle to be 250 and 1160 ppm, respectively. Estimation of the abundance of carbon compounds in the upper mantle from lavas is more difficult, because of potential loss of CO_2 during magma ascent. Various researchers have given estimates for CO_2 content in primitive mantle ranging between 230 and 550 ppm (Zhang & Zindler, 1993; Jambon, 1994). H_2O appears to be the most abundant among volatile species in the upper mantle. The abundances of carbon and H_2O in normal mantle are low enough that they may be stored entirely within minerals. With mantle upwelling and decompression, volatile components may be released either by dissociation reactions or by exsolution from nominally anhydrous minerals.

Oxygen fugacity imposes important controls upon the speciation of volatiles in vapor coexisting with lherzolite (Deines, 1980; Ryabchikov, 1988). Under relatively oxidized conditions, H_2O and CO_2 are prevailing compounds. Under reducing conditions, mixtures of (H_2O + CH_4) and (CH_4 + H_2) become stable (Ryabchikov, 1988). The oxidized nature of uppermost mantle vapors is consistent with commonly observed fluid microinclusions captured by the minerals of spinel lherzolites and filled with dense CO_2. Larger (up to several centimeters) segregations of dense CO_2 have been discovered (Kovalenko *et al.*, 1987). Schrauder & Navon (1993) found solid CO_2 inclusions in diamond, and the major volatile species in fluid microinclusions in coated diamonds (Navon *et al.*, 1988) are H_2O and CO_2 in carbonate material. All these facts suggest that down to the base of continental lithosphere carbon and hydrogen should be present in mantle fluids predominantly as oxidized species (Haggerty, 1990; Wood *et al.*, 1991).

SYSTEM LHERZOLITE–CO_2–H_2O: VAPOR AND LIQUID COMPOSITIONS

Figure 1a shows the effect of oxidized vapors (CO_2 + H_2O) on the solidus of mantle lherzolite, extrapolated deeper than ~120 km by comparison with lherzolite–H_2O. For details of the phase diagram and reference citations, the reader is referred to Wyllie (1979, 1987*a*, 1995, fig. 6), Olafsson & Eggler (1983), Wallace & Green (1988), and Falloon & Green (1990). CO_2 is stored in subsolidus dolomite or magnesite at depths greater than ~70 km and ~100 km, respectively. H_2O is stored in amphibole at depths less than ~90 km, and in phlogopite (given sufficient potassium) to somewhat deeper levels. At depths greater than ~300 km, H_2O is stored in dense hydrous magnesian silicates (DHMS, including wadsleyite), and perhaps brucite. The solidus curve, and liquid and vapor compositions, are buffered at depths greater than ~100 km by the formation of subsolidus carbonate, which yields carbonate-rich liquid at the solidus; any coexisting vapor phase is consequently enriched in H_2O (Wyllie, 1978; White & Wyllie, 1992).

Experimental measurements of the solubilities of silicate components in H_2O and (H_2O + CO_2) vapors at pressures and temperatures typical for the upper mantle (Nakamura & Kushiro, 1974; Ryabchikov & Boettcher, 1980; Ryabchikov *et al.*, 1982; Edgar & Arima, 1984; Ryabchikov & MacKenzie, 1985; Schneider & Eggler, 1986; McNeil & Edgar, 1987) show that the results are strongly dependent on mineralogy (e.g. the $MgO–SiO_2–H_2O$ system, Nakamura & Kushiro, 1974; Ryabchikov *et al.*, 1982). The SiO_2 content of the vapor phase reaches ~35 wt % at 3 GPa, 1100°C, whereas Mg_2SiO_4 solubility remains low. Even higher concentrations of solutes were revealed for alkali silicates and aluminosilicates in aqueous vapors equilibrated with omphacitic pyroxenes and micas (Ryabchikov & Boettcher, 1980; Ryabchikov *et al.*, 1982). The total concentration of silicates in the aqueous phase coexisting with phlogopite and forsterite at 1100°C and 3 GPa amounts to ~50 wt %. As a result of the higher solubility of potassium compounds in the join $NaAlSi_2O_6–KAlSi_3O_8–H_2O$, at 2 GPa and 700°C the silicate content in the vapor increases from ~30 wt % in the $NaAlSi_2O_6–H_2O$ boundary system to ~60% for vapor coexisting with both jadeite and muscovite (Ryabchikov & Ganeev, 1990). Schneider & Eggler (1986) found lower solubilities of silicate compositions, and reported that the addition of moderate amounts of CO_2 to H_2O caused drastic reduction of silicate solubilities. We have not found so drastic a reduction caused by CO_2 addition to H_2O.

Figure 2 summarizes experimental results showing the compositions of liquids coexisting with model peridotite assemblages containing CO_2, from 1 to 6 GPa. Liquidus

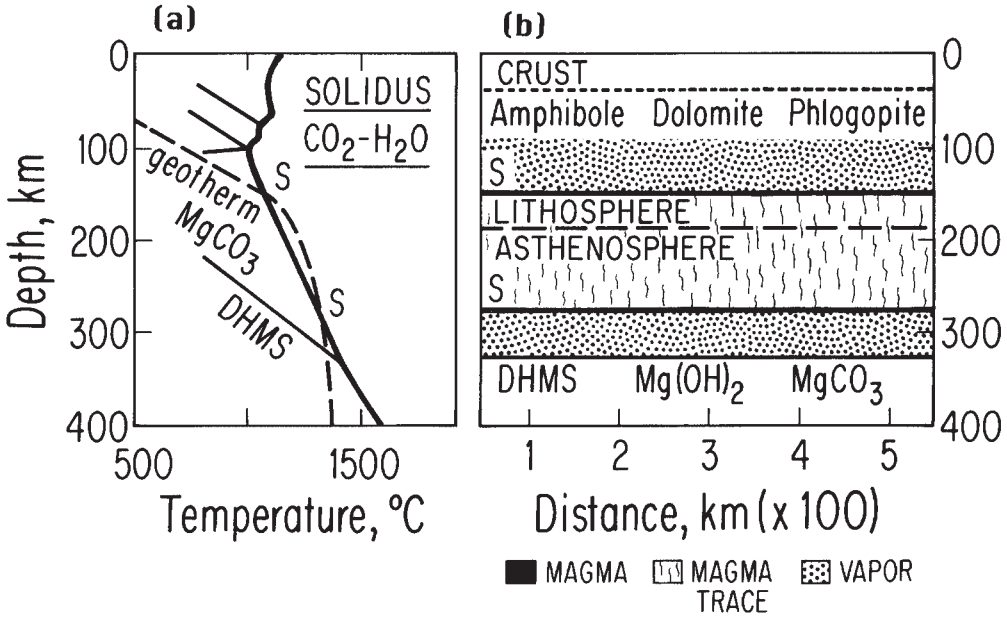

Fig. 1. (a) Solidus for lherzolite–CO_2–H_2O (bold continuous line) extrapolated from experimental data mainly <3·5 GPa (~110 km depth), and selected subsolidus phase boundaries (fine lines). The subsolidus phase relationships at >100 km depth are not relevant for the current problem, and are too complex for treatment here. Sources are given in the text (DHMS is 'dense hydrated magnesian silicate', and several minerals have now been identified, including wadsleyite, which introduce additional phase boundaries within this deep field). The dashed line is a hypothetical geotherm to illustrate intersections with phase boundaries. The geotherm exceeds the solidus temperature at depths between the intersection points S and S, and intersects the DHMS phase boundary at ~310 km. (b) For the geotherm shown, and with lherzolite containing evenly distributed traces of H_2O and CO_2, the three intersection points in (a) provide the three isobaric phase boundaries in the mantle cross-section (b). A trace of liquid occurs between the boundaries S and S, and vapor (dotted) is present above and below the partially melted zone. At depths below the DHMS phase boundary at ~320 km, all H_2O and CO_2 is stored in DHMS and magnesite. In reality, volatile components would be irregularly distributed, and vapors and liquids would migrate.

field boundaries for mostly vapor-saturated mineral assemblages have been projected from CO_2 onto the triangle CaO–MgO–SiO_2. The field boundaries subparallel to the carbonate join (CaO–MgO) give the compositions of the carbonate-rich liquids generated from carbonate–silicate assemblages, which increase in Mg/Ca with increasing pressure. Calcite–wehrlite yields liquid F′ at 1 GPa (Lee & Wyllie, 2000). Dolomite–lherzolite yields liquid F at 2·7 GPa, approaching DP at 3 GPa (Wyllie & Lee, 1998; Lee *et al.*, 2000), and liquid DP at 6 GPa (Dalton & Presnall, 1998*a*, 1998*b*, with Al_2O_3 added). With rising temperature and melting of carbonate, liquid compositions follow the field boundaries toward the silicate assemblage (e.g. F–B at 2·7 GPa), or subparallel vapor-absent boundaries (Dalton & Presnall, 1998*b*; Moore & Wood, 1998; Wyllie & Lee, 1998). These model-system results are supported by experiments with various CO_2-bearing peridotites (Wallace & Green, 1988; Ryabchikov *et al.*, 1989, 1993; Thibault *et al.*, 1992; Dalton & Wood, 1993; Sweeney, 1994). Carbonated mantle between 70 and 200 km depth yields a dolomitic partial melt; we anticipate that this conclusion will persist down to at least 400 km, and probably to much greater depths. The composition fields shown for various rock types indicate their positions with respect to the liquidus field boundaries at various pressures showing their possible relationship to CO_2-bearing melts, but further discussion is impossible in this paper; details and petrogenetic considerations were offered by Lee & Wyllie (2000).

The effects on the phase relationships of adding H_2O to CaO–MgO–SiO_2–CO_2 were examined by Wyllie (1978, 1979), and White & Wyllie (1992). The solidus temperature is lowered (Olafsson & Eggler, 1983; Wallace & Green, 1988; Falloon & Green, 1990), but the near-solidus partial melts remain carbonate rich, and H_2O either simply dissolves in the melt or, if in sufficient quantity, it is concentrated into a coexisting aqueous vapor phase.

Figure 3 shows four solidus curves for mantle peridotite. The dashed line is the volatile-free solidus measured by Takahashi (1986). The C–H curve represents the solidus under very reduced conditions, estimated on the basis that CH_4–H_2 lowered the solidus temperature in a model system by 85°C at 2·8 GPa (Green *et al.*, 1987), which corresponds rather closely to the $a_{H_2O} = 0{\cdot}35$ curve on the solidus for reduced lherzolite–volatiles reported by Taylor & Green (1988). The solidus for lherzolite–H_2O is measured to 6 GPa (Kushiro *et al.*, 1968) and

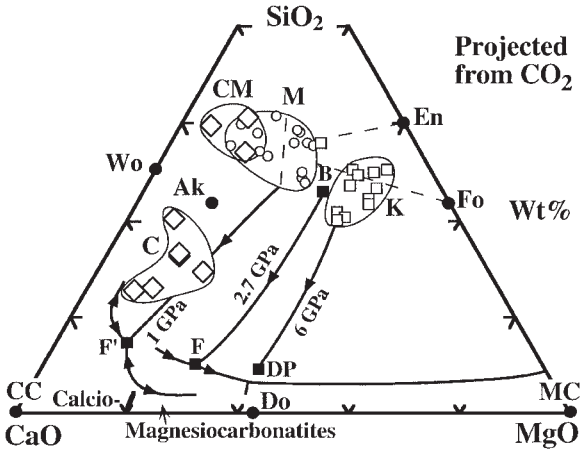

Fig. 2. Vapor-saturated liquidus field boundaries (bold lines with arrows showing falling temperatures) for various pressures projected from CaO–MgO–SiO_2–CO_2 onto the CO_2-free triangle, compared with projected rock compositions (after Lee & Wyllie, 2000). Mantle peridotites and mafic magmas (basalt–picrite) project within the triangle Fo–En–Di (dashed lines, Di behind area M). The compositions of selected rock types occupy the areas K (kimberlite, □), M (melilitite, ○), CM (carbonatite–melilitite, ◇), and C (carbonatite, also ◇). The first liquids generated from carbonated peridotites at various pressures are carbonatitic with compositions such as F′, F or DP. With progressive melting, liquids follow the field boundaries toward the silicate assemblage (e.g. F–B at 2·7 GPa). The relationship between these paths and the areas of projected rock types is discussed elsewhere (Lee & Wyllie, 2000). CC, calcite; Do, dolomite; MC, magnesite; Fo, forsterite; En, enstatite; Wo, wollastonite; Ak, akermanite.

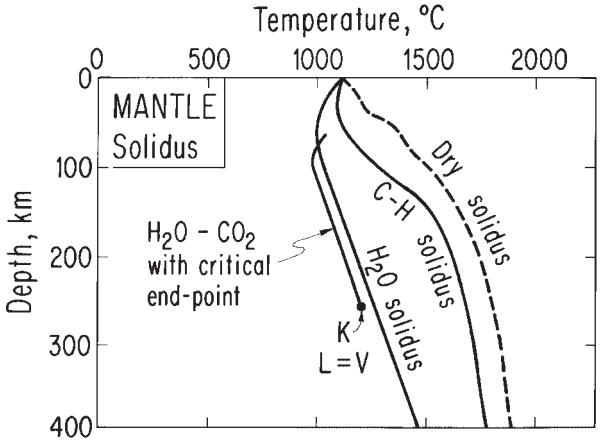

Fig. 3. Four solidus curves for lherzolite, with and without volatile components. (See text for explanation, and sources for each curve.)

interpolated to an experimental point at ~650 km, 1550°C (Thompson, 1992); Ryabchikov (1988) predicted the occurrence of a critical end-point on the solidus for peridotite–H_2O between 3 and 4 GPa, on the basis of experiments in simpler systems. The curve for lherzolite–H_2O–CO_2 is from Fig. 1, at pressures >2 GPa where the lherzolite becomes carbonated. Wallace & Green (1988) located the solidus below that for lherzolite–H_2O in the 2–3 GPa range, and this arrangement is assumed to persist in the extrapolation. The solidus is shown terminating at a hypothetical critical end-point K, placed arbitrarily at 250 km to illustrate the nature of phase relationships in mantle cross-sections with graphical clarity. As indicated below, a critical end-point may exist at shallower depths (minimum 125 km).

MAGMAS, VAPORS, AND CRITICAL FLUIDS

Kennedy *et al.* (1962) were the first to determine experimentally a second critical end-point of magmatic interest, on the solidus of the system SiO_2–H_2O at 0·97 GPa and 1080°C, but until recently there were few experimental data on other silicate–H_2O systems. The problem has been opened up by the experiments of Shen & Keppler (1997) and Bureau & Keppler (1999), who reported direct visual observations of miscibility between silicate melts and water in externally heated diamond-anvil cells. They suggested that there is complete miscibility between silicate melts and water in most of the upper mantle. The geometry of relationships between solidus curves and first and second critical end-points (K_1 and K_2) was illustrated by Wyllie & Tuttle (1960) in detailed phase diagrams around the hypothetical end-points in the system albite–H_2O, on the basis of limited experimental data. They assumed P–T values near 0·8 GPa and 750°C for K_2, but in subsequent experiments in the system $NaAlSiO_4$–SiO_2–H_2O to 3·5 GPa, Boettcher & Wyllie (1969*b*) measured the solidus for albite–H_2O compositions to pressures above the albite–jadeite transition without detection of critical phenomena. However, Goldsmith & Jenkins (1985) reported anomalous features in albite–H_2O experiments suggestive of critical relations near 1·4 GPa, and Paillat *et al.* (1992) calculated from solubility measurements that K_2 should occur near 1·6 GPa on the albite–H_2O solidus. The recent results of Shen & Keppler (1997) and Bureau & Keppler (1999) using the new techniques indicate that K_2 for the albite–H_2O solidus should occur in the rather complex region of the albite–jadeite transition, between 1·5 and 1·7 GPa near 625–650°C, and that K_2 for the jadeite–H_2O solidus is near 1·8 GPa and 700°C. Schreyer (1999) presented a detailed analysis and interpretation of the old and new experiments for hydrothermal albite and jadeite + quartz melting reactions.

In mantle-related systems, Boettcher & Wyllie (1969*a*) located a critical end-point on the solidus for CaO–SiO_2–CO_2–H_2O at 3·25 GPa and 515°C, for a reaction involving a hydrated Ca-silicate, calcite, portlandite, liquid and vapor (addition of MgO provides the model

lherzolite–CO_2–H_2O system). They also illustrated possible relationships between the critical curve for a system and the critical end-points for different mineral assemblages within the system. Solubilities close to 50 wt % of solid components in the vapor phase in the join phlogopite–forsterite–H_2O at 3 GPa and 1100°C (Ryabchikov & Boettcher, 1980) suggest that a critical end-point may occur at a pressure somewhat above 3 GPa. Ryabchikov (1988) projected, from simple systems, the isolines of total silicate contents in vapors and coexisting silicate melts onto the pressure–temperature diagram for lherzolite–H_2O (which includes traces of phlogopite and sodium-bearing clinopyroxenes). This diagram, based on extrapolations, gave the estimated position of a critical end-point between 3 and 4 GPa, at ~1050°C, and with silicate content in the vicinity of 60 wt % of the critical fluid.

The effect of small compositional variations in complex rocks was illustrated by Bureau & Keppler's (1999) experiments on critical curves for H_2O with haplogranite and calkalkaline granite. Schreyer (1999) compared the old and new experiments for haplogranite, presenting also new measurements of phase compositions in high-pressure granite–H_2O experiments. Our extrapolations of the new critical curves to solidus curves indicate K_2 between 2·5 and 3 GPa for haplogranite–H_2O (Huang & Wyllie, 1975), and between 4 and 5 GPa for calcalkaline granite–H_2O (Boettcher & Wyllie, 1968; Stern & Wyllie, 1981), with more uncertainties in the latter extrapolation. These estimated ranges for K_2 correspond to depths of 80–100 km and 125–150 km, respectively. The small differences in composition between haplogranite and calcalkaline granite thus appear to be associated with depth differences for K_2 between 25 and 70 km.

Although a critical end-point on the solidus for lherzolite–CO_2–H_2O has not been measured experimentally, the evidence reviewed above is strongly suggestive for its existence. The probable effect of CO_2 through reduction of dissolved constituents in the vapor phase (Schneider & Eggler, 1986) would be to shift K_2 to pressure higher than for lherzolite–H_2O. The position of K in Fig. 3 at 250 km (~7·5 GPa) is arbitrary, located for graphical clarity of the phase relationships to be illustrated, but it is not inconsistent with other results; its depth would vary with peridotite composition (Bureau & Keppler, 1999).

The relationships between rock, magma and volatile components at depths shallower than and deeper than K_2 are illustrated in the schematic isobaric sections of Fig. 4. These are two-dimensional slices through a multicomponent system, and phase compositions do not lie on the joins; but the phase fields intersected show the phase changes experienced by any bulk composition on a join 'solids–volatiles'; 'solids' may represent any rock composition, and 'volatiles' may represent any combination of volatile components. The precise positions of phase boundaries obviously vary with rock–volatile composition, but the topology remains the same.

At depths shallower than K (Figs 3 and 4a), the solidus for melting in the presence of a vapor phase is essentially isothermal. At low pressures the amount of dissolved volatile components in the liquid is limited to a few percent, and the amount of silicate components dissolved in the vapor phase is trivial; the compositions of liquid and vapor are separated by the large phase element for (L + V). With increasing pressure, the solubilities in both phases increase, represented by expansion of their phase fields in Fig. 4a as the size of (L + V) decreases. The composition of the liquid thus approaches that of the coexisting vapor (Wyllie, 1979, fig. 18; Boettcher & Wyllie, 1969*b*, fig. 10). If the two phases become equal in composition and properties, they merge into a single critical fluid phase and the solidus curve terminates at a second critical end-point, the point K on the solidus curve in Fig. 3. At this point, either the (L + V) phase element shrinks to a vanishing point on the liquidus [as determined by Bureau & Keppler (1999) for their compositions], or it separates from the liquidus and migrates to higher temperature (off the top of Fig. 4; Wyllie & Tuttle, 1960, fig. 4C). The result as shown in Fig. 4b is that there is a continuous transition from vapor phase to liquid through a critical fluid, with no phase boundaries between. Therefore, at pressures greater than K there is no solidus phase boundary where the vapor dissolves into a liquid phase. The black band for 'rock melts' represents the melting interval of the volatile-free rock (above the 'dry solidus' of Fig. 3).

For lherzolite–CO_2–H_2O at high pressures, the near-solidus liquid is carbonatitic (with silicate content increasing with rising temperature; see Fig. 2), and any coexisting vapor is aqueous (Wyllie, 1978; White & Wyllie, 1992), with wide separation between their compositions as in Fig. 4a. At pressures greater than K, Fig. 4b shows that with rising temperature the rock would coexist with aqueous vapor, with a fluid phase varying continuously between an aqueous vapor and carbonate-rich liquid, reaching a dolomitic composition, and then carbonate–silicate liquids that approach normal mafic liquids ('rock melts'). The higher-temperature liquid compositions are represented by paths corresponding to F–B and subparallel paths in Fig. 2. The phases in Fig. 4 labeled 'liquid' and 'vapor' are both fluids in a physical sense, but the diagrams illustrate the reason for distinguishing between the terms liquid, vapor and fluid when dealing with volatile components at mantle pressures, where critical phenomena may intervene (Wyllie, 1987*b*).

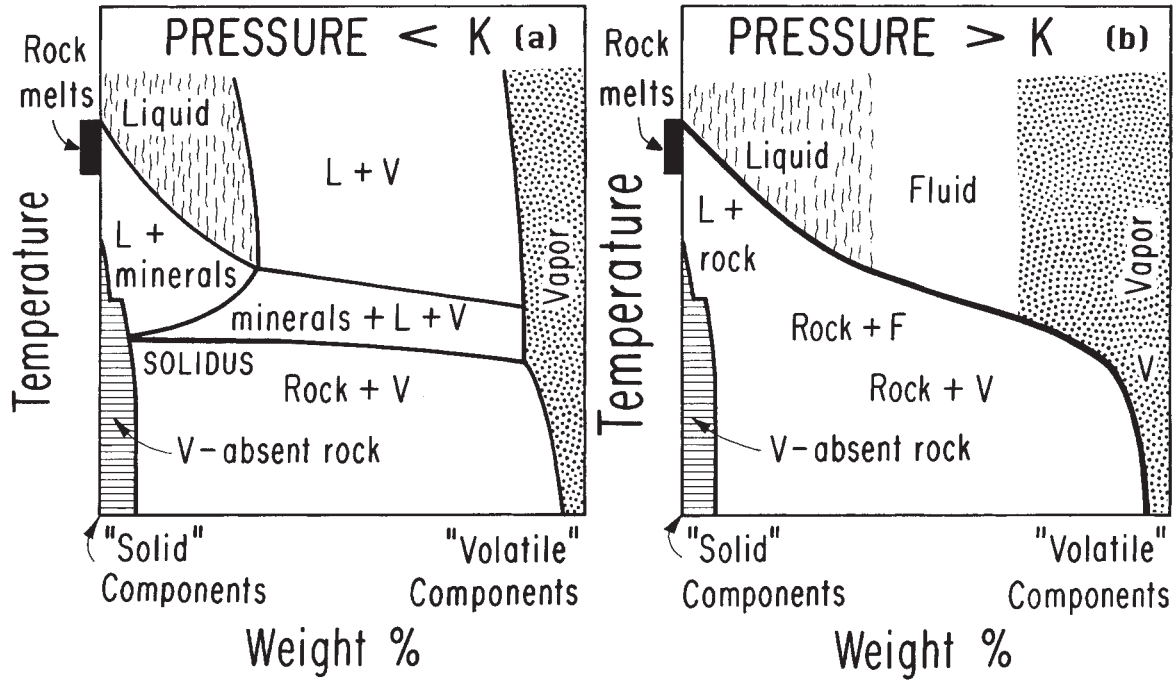

Fig. 4. Generalized system 'solid–volatile components': two-dimensional slices through complex systems, representing any rock–volatile system, in particular lherzolite–H_2O–CO_2. Isobaric phase relationships at levels shallower than and deeper than K (Fig. 3). Shading as in Figs 1 and 5–7. The narrow, high-temperature melting interval for volatile-free rock should be noted; this interval yields basaltic and picritic magmas from lherzolite. With addition of volatile components, the liquidus temperature is depressed. The fields for vapor-absent rock should be noted: this field includes nominally anhydrous rocks with H_2O or C dissolved in minerals. With rising temperature or decreasing pressure, the solubility decreases, and H_2O (or species of C) may be exsolved from the minerals. These are not binary diagrams: phase compositions do not lie on the rock–volatile composition join. (a) At pressures below the critical end-point, K, the compositional ranges of liquid and vapor are distinct, and physically separated by the field (L + V). With CO_2 at depths greater than ~100 km (Fig. 1a) the low-temperature liquid is carbonatitic, near dolomite composition (e.g. F in Fig. 2), and any coexisting vapor is aqueous. With rising temperature, the liquid changes through carbonate–silicate compositions toward various low-SiO_2 rock compositions (Fig. 2). (b) At higher pressures above K (Fig. 3), there is a continuous fluid phase (F) connecting the higher-temperature carbonatite liquid (L) and the lower-temperature aqueous vapor (V). There are no phase boundaries between L and V, and there is no defined solidus where melting begins.

GEOTHERMS, SOLIDUS CURVES AND MANTLE PLUMES

Phase assemblages in the mantle vary according to the bulk-rock composition and geotherms. Figure 1a compares selected phase boundaries for lherzolite–CO_2–H_2O with a hypothetical geotherm drawn to illustrate three intersections with phase boundaries: two points S where the geotherm crosses the solidus, and the point where it crosses the phase boundary for DHMS. These intersection points occur as horizontal phase boundaries in the mantle cross-section of Fig. 1b. For lherzolite containing evenly distributed traces of H_2O and CO_2, in excess of those dissolved in nominally anhydrous minerals, the mantle would be mineralogically zoned as shown in Fig. 1b. Volatile components are stored in minerals in the uppermost mantle (amphibole, dolomite, phlogopite), and in mantle deeper than ~300 km (DHMS, magnesite, brucite). The subsolidus phase relationships at depth less than ~100 km are too complex to be treated in detail here. In the depth interval S–S, where the geotherm exceeds the solidus, a trace of liquid (composition dolomitic) is formed and dissolves all volatile components (except for a narrow temperature interval above the solidus where a trace of free vapor may persist). There are zones above and below the partially melted zone with a separate (H_2O + CO_2) vapor phase (dotted areas). In reality, the volatile components would be irregularly distributed, and both vapors and liquids would migrate (Wyllie, 1987*a*, 1995, fig. 7), with migration controlled by dihedral angles and other properties (e.g. Minarick, 1998).

Figure 5a shows selected lherzolite–CO_2–H_2O phase boundaries, and Fig. 5b represents a cross-section beneath the oceanic lithosphere, with the mantle initially volatile free. Instead of a single geotherm as in Fig. 1a, let us consider a thermal plume with isotherms in standard mushroom-shape arrangement (Courtney & White, 1986; White & McKenzie, 1989; Watson & McKenzie, 1991), which provides a series of geotherms at higher

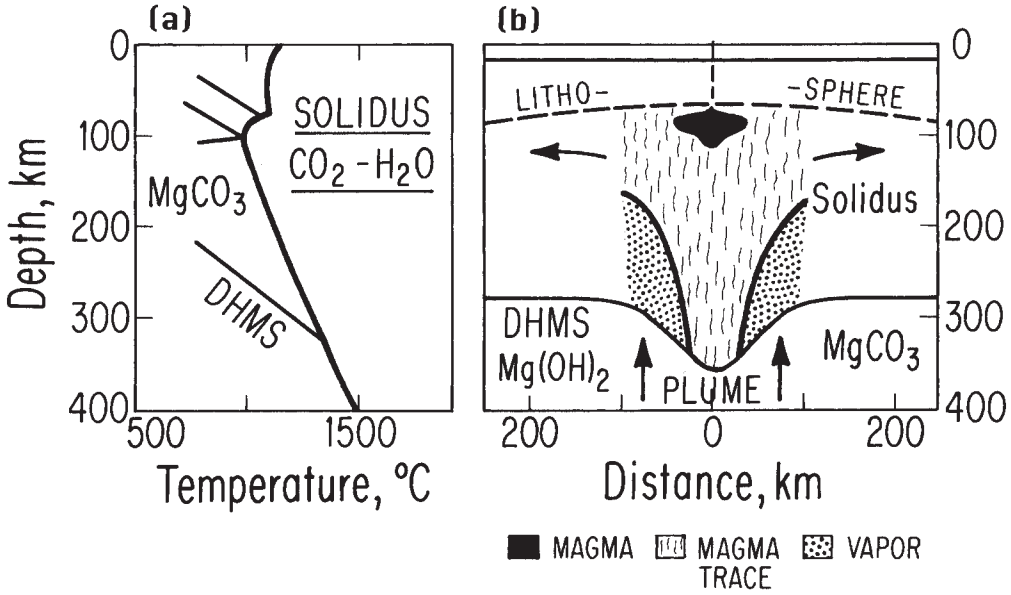

Fig. 5. (a) The solidus and selected reactions for lherzolite–CO_2–H_2O (slightly modified from Fig. 1a), without intervention of critical phenomena. Instead of a single geotherm as in Fig. 1a, we consider a thermal plume with isotherms in standard mushroom arrangement. The thermal structure adopted is that used by Wyllie (1988, fig. 4), based on the quantitative study of Courtney & White (1986). More comprehensive treatments include those of White & McKenzie (1989) and Watson & McKenzie (1991). With this thermal structure, each location has a different geotherm, with temperatures rising from margin to center of the plume. (b) Phase fields intersected in a mantle cross-section based on intersection points between the phase boundaries in Figs 3 and 5a, and the series of geotherms associated with a mantle plume. (See text for description.) The plume above the 300 km level becomes a cylinder containing traces of carbonate-rich and carbonate–silicate liquids, with an outer sheath containing aqueous vapor, and a small shallow kernel containing mafic silicate magma. The topology is defined, but the geometry varies with thermal structure and phase boundaries (which vary with bulk composition, or in volatile components). Shading as in Figs 1, 4, 6, and 7.

temperatures for successive positions approaching the central axis. We assume that H_2O and CO_2 rise through the mantle along with plume material. Two phase boundaries from Fig. 5a are mapped in Fig. 5b in terms of the P–T points defined on isotherms, using the specific thermal structure from Wyllie [1988, fig. 4; based on quantitative treatment by Courtney & White (1986)]: the dissociation phase boundary (DHMS) near 300 km depth, and the solidus. The solidus, instead of being near-horizontal as in Fig. 1b, curves down steeply to deeper levels toward the plume axis, as the deeper intersection of solidus–geotherm S in Fig. 1a migrates to greater depths with rising geotherm temperature. Near the center of the plume, the high-temperature geotherms intersect the 'dry solidus' of Fig. 3 in pairs of points (compare S–S for the volatile–solidus in Fig. 1a), and these points enclose the small black area designated 'magma', where mafic melt is generated even in the absence of volatile components. We emphasize that this is a schematic diagram, with correct topology but with geometry varying according to variations in isotherms and phase relationships (bulk composition).

At either side of the mantle cross-section, with lower temperatures and no volatile components, neither vapor nor liquid is present. A rising mantle plume reacts as it crosses the DHMS phase boundary, releasing H_2O and CO_2 stored in minerals and forming an aqueous vapor phase in the outer annular ring of the plume (Wyllie, 1988). As the vapor rises with or through the plume, it reaches the solidus; as the vapor crosses the bold line (compare the solidus in Fig. 4a) it dissolves into a trace of vapor-undersaturated dolomitic liquid (e.g. DP, Fig. 2). The center of the plume is hot enough (in this example) that the dissociating volatile components pass directly from the vapor-absent rock into the vapor-absent dolomitic liquid. The plume above the 300 km level thus becomes a cylinder containing traces of carbonate-rich and carbonate–silicate liquids, with an outer sheath of aqueous vapor, and a small shallow kernel of silicate magma (mafic, basaltic–picritic).

If the solidus in Fig. 5 has a critical end-point (Fig. 3), the consequences are as shown in Fig. 6. The phase fields in the mantle cross-section remain unchanged at depths shallower than K, and at depths deeper than the DHMS phase boundary. The bold solidus curves S (Fig. 6b), however, terminate at the depth–temperature value of the critical point. The locus of the point K from Fig. 6a traces a constant-depth circle within the plume of Fig. 6b, and the zone of fluid (F, white, between shaded areas) extends deeper from that ring in the shape of a hollow cylinder, separating the outer cooler zone with aqueous vapor (dotted) from the inner hotter zone with

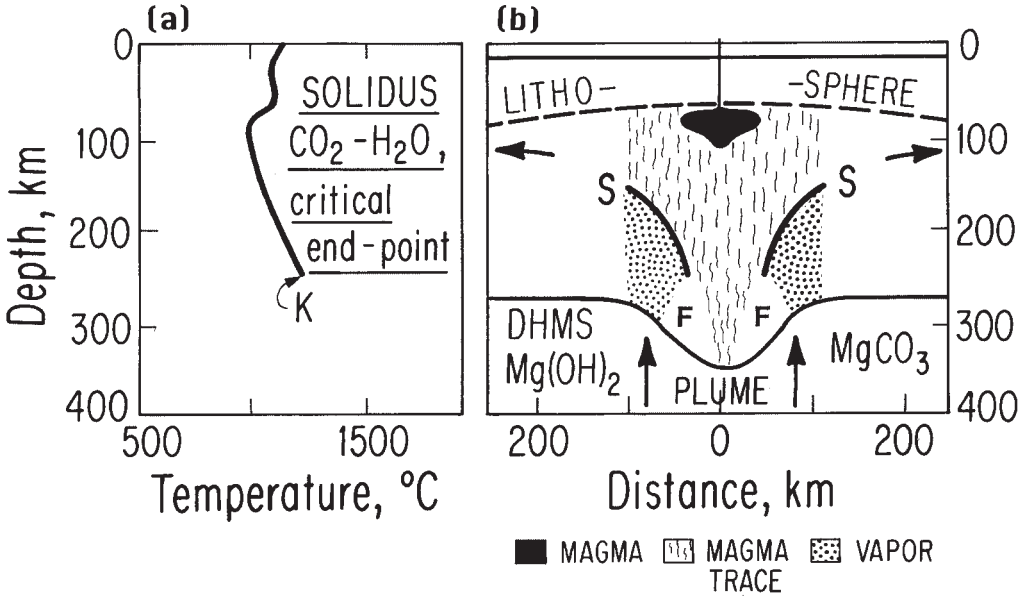

Fig. 6. (a) The solidus for lherzolite–CO_2–H_2O assuming that there is a critical end-point, K, on the solidus of Fig. 5a, located arbitrarily at 250 km, as in Fig. 3. Adopted geotherms are for a thermal plume, the same as in Fig. 5. (b) Phase fields intersected in a mantle cross-section with a plume, as in Fig. 5b, with the difference that at K the liquid becomes critically identical with vapor, and the bold solidus curves S cease to exist at greater depths. Deeper than K, cooler aqueous vapor (dotted) in the outer plume changes continuously without phase boundaries through intermediate fluid (F) to carbonatitic liquid in the hotter center of the plume. The complete range of materials from carbonatitic liquid (L) through supercritical fluid (F) to aqueous vapor (V) as illustrated in Fig. 4b occurs within a small volume of mantle at levels somewhat deeper than K. Shading as in Figs 1, 4, 5, and 7. [From Wyllie (1995).]

a trace of dolomitic melt. The isobaric phase diagram, Fig. 4b, illustrates this progressive change with rising temperature. The complete range of fluid materials from aqueous vapor through supercritical fluid to carbonatite liquid occurs within a small volume of mantle at levels somewhat deeper than K (Fig. 6). At depths shallower than K, aqueous vapor and carbonatitic liquid can coexist at the solidus S, but between K and the deeper DHMS phase boundary, aqueous vapor and carbonatitic liquid cannot coexist, as shown by Fig. 4b. The topology of the phase fields in the mantle cross-section of Fig. 6b provides a guide for mantle processes. The precise geometry may vary as stated above; in particular, the depth of K may vary with volatile components.

For mantle containing no volatile components, there is no vapor and no melting at depths >100 km in Fig. 6b. The only phase boundary remaining is that around the small black area where mafic magma is generated. For mantle containing only the volatile components dissolved in nominally anhydrous minerals (Bell & Rossman, 1992), there is no vapor and no melt unless the upwelling mantle reaches a depth where the minerals exsolve these components. The field for 'vapor-absent rock' in Fig. 4 includes hydrates and carbonates as well as the nominally anhydrous minerals with dissolved H_2O and C. With rising temperature (Fig. 4) or decreasing pressure (Figs 5 and 6), the solubility of dissolved volatile components in minerals decreases, and H_2O and species of C may be exsolved. The exsolved components will generate either a vapor phase or a trace of melt, depending on position within the phase fields of Figs 4, 5b or 6b when exsolution occurs. The consequence of this process was described by Hirth & Kohlstedt (1996), who estimated that exsolution of H_2O would cause partial melting to begin near 115 km depth.

For mantle with low oxygen fugacity, the relevant solidus is at relatively high temperature, as shown in Figs 3 and 7a. Assuming that the reduced condition precludes the presence of hydrates or carbonates, there is no DHMS boundary, and the mantle cross-section in Fig. 7b shows reduced vapor (dotted) rising with the plume to a shallow solidus (S–S). There is only a narrow zone of partial melt generated around the black area corresponding to volatile-free melting. Reduced vapors rising as in Fig. 7b may enter a more oxidized upper mantle, which causes an effective lowering of the solidus (Fig. 3) with resultant partial melting (Wyllie, 1980). This process was elaborated in elegant detail by Green *et al.* (1987) as 'redox melting'.

APPLICATIONS

Carbonate- and water-rich fluids found in fibrous diamonds are believed to be representative of the fluids

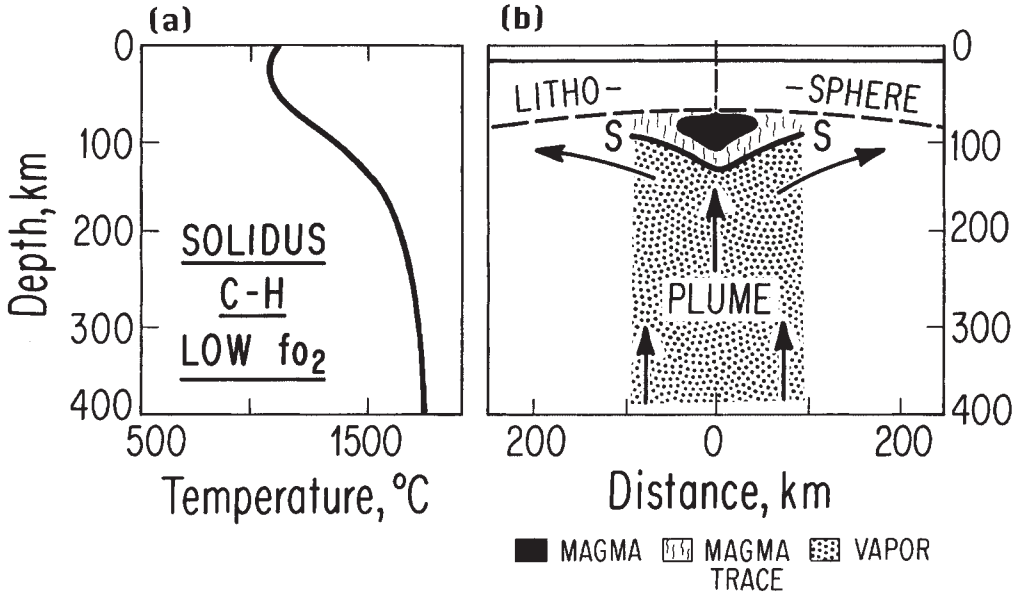

Fig. 7. (a) The solidus for lherzolite–C–H under very reduced conditions [based on Taylor & Green (1988); see text with Fig. 3]. Adopted geotherms are for a thermal plume, the same as in Figs 5 and 6. (b) Phase fields intersected in mantle cross-section with plume, as in Figs 5b and 6b, with the difference that there are no hydrated or carbonated minerals, and no oxidized vapor phase. The solidus S–S shifts to much shallower levels than in Figs 5b and 6b. Shading as in Figs 1 and 4–6.

from which the diamonds grew. The bulk composition of the microinclusions in individual diamonds defines a tight compositional range (Schrauder & Navon, 1994), suggesting that mineral phases now found in the inclusions were fully dissolved in the fluid at mantle temperature. However, fluids in 13 diamonds from Jwaneng, Botswana, span a continuous range of compositions between a hydrous end-member, dominated by SiO_2 (50–60%) and K_2O (10–20%), and a carbonatitic end-member with (CaO + FeO + MgO) >80% and CaO > (MgO + FeO), which is also rich in K_2O. Trapping pressures of 4–7 GPa (125–210 km) were estimated from the IR shift of secondary quartz and the equation of state of pure water (Navon, 1991). Schrauder & Navon (1994) proposed three models for the evolution of the fluids: transition from hydrous to carbonatitic composition during heating, the reverse path during cooling and crystallization or mixing of the two end-members. They favored the second alternative and further suggested that these fluids may have evolved from an earlier kimberlite-like fluid by cooling and crystallization of silicate minerals followed by carbonate crystallization during the growth of the diamonds.

We consider the end-member analyses reported by Schrauder & Navon (1994) to be consistent with the expected carbonatite liquids and aqueous vapors produced in peridotite (Fig. 2; White & Wyllie, 1992). At depths greater than the critical end-point (K, Fig. 6a), the intermediate fluid compositions in Fig. 4b probably show a near-linear relationship between the liquid and vapor end-members, corresponding to that observed in diamonds. Each diamond would grow from a fluid whose composition is defined by the depth and temperature; a group of diamonds growing within a limited mantle volume at depths greater than K could trap samples of any one of the critical fluids (F) between the dolomitic liquid and SiO_2-rich hydrous vapor. We conclude that the analyses by Schrauder & Navon (1994) provide strong supporting evidence for the existence of a critical end-point for lherzolite–H_2O–CO_2 at some depth in the upper mantle >125 km (Ryabchikov, 1988; Navon, 1991).

In Figs 5b, 6b and 7b we present a picture of mantle plumes rising with traces of interstitial vapor, which may be transported from great depths, or which may be released by dehydration (possibly combined with decarbonation) reactions at a depth of ~300 km. The vapor becomes dissolved in a trace of interstitial volatile-rich liquid when it reaches the solidus phase boundary (S–S), the geometry of which varies, depending on the details of the thermal structure of the plume and the oxygen fugacity (Figs 3 and 7).

Both vapor phase and volatile-rich magma are enriched in incompatible elements (e.g. Mysen, 1978). The partition coefficients of trace elements between rock and vapor will in general differ from those between rock and silicate melt. Therefore, the distribution of trace elements in the dynamic systems will change as the plume crosses the solidus boundary. In addition, the partition coefficients vary as a function of pressure at the solidus boundary (Blundy & Wood, 1994). Figures 5b and 6b

show the solidus boundary spanning >100 km, from >300 km depth near the center of a plume, to <200 km depth at its outer edge. The trace element patterns imposed at depth on the trace magmas in the sheaths around the major melting zones of plumes should thus vary radially from the plume center, according to the depth of the solidus phase boundary.

The trace magmas rising in the central part of the plumes enter the main melting regions (the black areas of the figures where geotherms are situated above the volatile-free solidus), and the incompatible trace elements are incorporated into the silicate magma generated there. However, there is an annular region around this melting region where the trace magmas rise directly into the lithosphere. At the outer margins, these trace melts are essentially dolomitic carbonatite magmas, grading through carbonate–silicate magmas in a zone surrounding the black regions for mafic magmas (picritic or basaltic). Watson & McKenzie (1991) have investigated the melting, uprise and freezing of the central silicate magmas.

In fact, the dynamics of a plume, and the relative movements of vapors, liquids and host rocks involving transfer of material and heat, will modify the idealized picture. Experimental data related to crystal–liquid partition coefficients, and the connectivity, mobility and migration of volatile-rich fluids were summarized by Wyllie (1995). The behavior of the liquid and its passage through the lithosphere to volcanoes is critically dependent on the fluid dynamics of the migration of liquid through a deforming rock matrix, the rheology and fracturing of the lithosphere, and the extent to which the melt re-equilibrates with the host rock during migration. These matters were addressed by White & McKenzie (1989) and Watson & McKenzie (1991).

Primary carbonate-rich melts entering the lithosphere in the marginal parts of mantle plumes (Figs 5 and 6) or from cooler parts of the mantle (e.g. Fig. 1b) may be very efficient agents of metasomatism (Green & Wallace, 1988; Ryabchikov *et al.*, 1989). Phase equilibrium data bearing on the reactions associated with such processes at depths of ~70–100 km have been reviewed and applied by Wyllie (1980), Dalton & Wood (1993), Moore & Wood (1998) and Lee & Wyllie (2000).

The upward migration of these vapors and trace magmas should result in the redistribution of mobile elements within the mantle, thus metasomatizing the mantle and 'preparing' sources capable of providing the geochemical signatures for kimberlites, lamproites and other types of alkaline primary magmas during subsequent melting events. An interesting feature of the fluids trapped by natural diamonds is the very high light/heavy rare earth element (LREE/HREE) ratios typical for them, which are comparable with REE patterns of lamproites and type II kimberlites (Schrauder *et al.*, 1996). If we assume that these fluids were in equilibrium with normal mantle minerals, then the difference between partition coefficients of LREE and HREE for such alkaline aqueous fluids should be much larger than for silicate melts or fluids without alkalis (Mysen, 1978). This demonstrates the potential importance of such highly alkaline fluids and vapors for geochemical differentiation in the mantle, inasmuch as the very steep REE patterns typical for lamproites and some peridotitic nodules are difficult to explain on the basis of the known values of partition coefficients for garnets and clinopyroxenes.

ACKNOWLEDGEMENTS

We thank G. Brey, H. Keppler, O. Navon, W. Schreyer, and M. Wilson for helpful comments. This research was supported by the Earth Science Section of the US National Science Foundation, Grant EAR-9218806. This is Contribution 8721 of the Division of Geological and Planetary Sciences, California Institute of Technology.

REFERENCES

Bell, D. R. & Rossman, G. R. (1992). Water in Earth's mantle: the role of nominally anhydrous minerals. *Science* **255**, 1391–1397.

Blundy, J. & Wood, B. J. (1994). Prediction of crystal–melt partition-coefficients from elastic-moduli. *Nature* **372**, 452–454.

Boettcher, A. L. & Wyllie, P. J. (1968). Melting of granite with excess water to 30 kilobars pressure. *Journal of Geology* **76**, 235–244.

Boettcher, A. L. & Wyllie, P. J. (1969*a*). The system CaO–SiO_2–CO_2–H_2O—second critical end-point on the melting curve. *Geochimica et Cosmochimica Acta* **33**, 611–632.

Boettcher, A. L. & Wyllie, P. J. (1969*b*). Phase relationships in the system $NaAlSiO_4$–SiO_2–H_2O to 35 kilobars pressure. *American Journal of Science* **267**, 875–909.

Bureau, H. & Keppler, H. (1999). Complete miscibility between silicate melts and hydrous fluids in the upper mantle: experimental evidence and geochemical implications. *Earth and Planetary Science Letters* **165**, 187–196.

Courtney, R. C. & White, R. S. (1986). Anomalous heat flow and geoid across the Cape Verde Rise: evidence for dynamic support from a thermal plume in the mantle. *Journal of Geophysical Research* **87**, 815–867.

Dalton, J. A. & Presnall, D. C. (1998*a*). Carbonatitic melts along the solidus of model lherzolite in the system CaO–MgO–Al_2O_3–SiO_2–CO_2 from 3 to 7 GPa. *Contributions to Mineralogy and Petrology* **131**, 123–135.

Dalton, J. A. & Presnall, D. C. (1998b). The continuum of primary carbonatitic–kimberlitic melt compositions in equilibrium with lherzolite: data from the system CaO–MgO–Al_2O_3–SiO_2–CO_2 at 6 GPa. *Journal of Petrology* **39**, 1953–1964.

Dalton, J. A. & Wood, B. J. (1993). The compositions of primary carbonate melts and their evolution through wallrock reaction in the mantle. *Earth and Planetary Science Letters* **119**, 511–525.

Deines, P. (1980). The carbon isotopic composition of diamonds: relationship to diamond shape, color, occurrence and vapor compositions. *Geochimica et Cosmochimica Acta* **44**, 943–961.

Edgar, A. D. & Arima, M. (1984). Experimental studies on K-metasomatism of a model pyrolite mantle and their bearing on the genesis of ultrapotassic magmas. *Proceedings 27th International Geological Congress 9*. Utrecht: VNU Science Press, pp. 509–541.

Falloon, T. J. & Green, D. H. (1990). Solidus of carbonated fertile peridotite under fluid-saturated conditions. *Geology* **18**, 195–199.

Goldsmith, J. R. & Jenkins, D. M. (1985). The hydrothermal melting of low and high albite. *American Mineralogist* **70**, 924–933.

Green, D. H. & Wallace, M. E. (1988). Mantle metasomatism by ephemeral carbonatite melts. *Nature* **336**, 459–462.

Green, D. H., Falloon, T. J. & Taylor, W. R. (1987). Mantle-derived magmas—roles of variable source peridotite and variable C–H–O fluid compositions. In: Mysen, B. O. (ed.) *Magmatic Processes: Physicochemical Principles. Geochemical Society Special Publication* **1**, 139–154.

Haggerty, S. E. (1990). Redox state of the continental lithosphere. In: Menzies, M. A. (ed.) *Continental Mantle*. Oxford: Clarendon Press, pp. 87–109.

Hirth, G. & Kohlstedt, D. L. (1996). Water in the oceanic upper mantle: implications for rheology, melt extraction, and the evolution of the lithosphere. *Earth and Planetary Science Letters* **144**, 93–108.

Huang, W. L. & Wyllie, P. J. (1975). Melting reactions in the system $NaAlSi_3O_8$–$KAlSi_3O_8$–SiO_2 to 35 kilobars, dry and with excess water. *Journal of Geology* **83**, 737–748.

Jambon, A. (1994). Earth degassing and large-scale geochemical cycling of volatile elements. In: Carroll, M. R. & Holloway, J. R. (eds) *Volatiles in Magmas. Mineralogical Society of America, Reviews in Mineralogy* **30**, 479–517.

Kennedy, G. C., Wasserburg, G. J., Heard, H. C. & Newton, R. C. (1962). The upper three-phase region in the system SiO_2–H_2O. *American Journal of Science* **260**, 501–521.

Kovalenko, V. I., Solovova, I. P., Ryabchikov, I. D., Ionov, D. A. & Bogatikov, O. A. (1987). Fluidized CO_2–sulphide–silicate media as agents of mantle metasomatism and megacryst formation: evidence from a large druse in a spinel-lherzolite xenolith. *Physics of the Earth and Planetary Interiors* **45**, 280–293.

Kushiro, I., Syono, Y. & Akimoto, S. (1968). Melting of a peridotite nodule at high pressures and high water pressures. *Journal of Geophysical Research* **73**, 6023–6029.

Lee, W. J. & Wyllie, P. J. (2000). The system CaO–MgO–SiO_2–CO_2 at 1 GPa, metasomatic wehrlites, and primary carbonatite magmas. *Contributions to Mineralogy and Petrology* **138**, 214–228.

Lee, W. J., Huang, W. L. & Wyllie, P. J. (2000). Melts in the mantle modeled in the system CaO–MgO–SiO_2–CO_2 at 2·7 GPa. *Contributions to Mineralogy and Petrology* **138**, 199–213.

McNeil, A. M. & Edgar, A. D. (1987). Sodium-rich metasomatism in the upper mantle: implications of experiments on the pyrolite–Na_2O-rich fluid system at 950°C, 20 kbar. *Geochimica et Cosmochimica Acta* **51**, 2285–2294.

Minarick, W. G. (1998). Complications to carbonate melt mobility due to the presence of an immiscible silicate melt. *Journal of Petrology* **39**, 1965–1973.

Moore, K. R. & Wood, B. J. (1998). The transition from carbonate to silicate melts in the CaO–MgO–SiO_2–CO_2 system. *Journal of Petrology* **39**, 1943–1951.

Mysen, B. O. (1978). Experimental determination of crystal–vapor partition coefficients for rare earth elements at 30 kbar pressure. *Carnegie Institution of Washington Yearbook* **77**, 689–695.

Nakamura, Y. & Kushiro, J. (1974). Composition of gas phase Mg_2SiO_4–SiO_2–H_2O at 15 kbar. *Carnegie Institution of Washington Yearbook* **73**, 255–258.

Navon, O. (1991). Infrared determination of high internal pressures in diamond fluid inclusions. *Nature* **353**, 746–748.

Navon, O., Hutcheon, I. D., Rossman, G. R. & Wasserburg, G. J. (1988). Mantle-derived fluids in diamond micro-inclusions. *Nature* **335**, 784–789.

Olafsson, M. & Eggler, D. H. (1983). Phase relations of amphibole–carbonate, and phlogopite–carbonate peridotite: petrologic constraints on the asthenosphere. *Earth and Planetary Science Letters* **64**, 305–315.

O'Neill, H. St C. & Palme, H. (1998). Composition of silicate Earth: implications for accretion and core formation. In: Jackson, I. (ed.) *The Earth's Mantle, Composition, Structure and Evolution*. Cambridge: Cambridge University Press, pp. 3–126.

Paillat, O., Elphick, S. C. & Brown, W. L. (1992). The solubility of water in $NaAlSi_3O_8$ melts: a re-examination of Ab–H_2O phase relationships and critical behaviour at high pressures. *Contributions to Mineralogy and Petrology* **112**, 490–500.

Ryabchikov, I. D. (1988). *Geochemical Evolution of Earth's Mantle* (in Russian). Moscow: Nauka, 37 pp.

Ryabchikov, I. D. & Boettcher, A. L. (1980). Experimental evidence at high pressure for potassic metasomatism in the mantle of the Earth. *American Mineralogist* **65**, 915–919.

Ryabchikov, I. D. & Ganeev, I. I. (1990). Isomorphous substitution of potassium in clinopyroxenes at high pressures (in Russian). *Geokhimiya* **1**, 3–12.

Ryabchikov, I. D. & MacKenzie, W. S. (1985). Interaction of jadeite with water at 20–30 kbar and 650°C. *Mineralogical Magazine* **49**, 601–603.

Ryabchikov, I. D. & Wyllie, P. J. (1991). The distribution and behavior of volatile components in the Earth's mantle. *IASPEI Program and Abstracts*, 169. 20th General Assembly, International Union of Geodesy and Geophysics, Vienna: Graz University of Technology.

Ryabchikov, I. D., Schreyer, W. & Abraham, K. (1982). Compositions of aqueous fluids in equilibrium with pyroxenes and olivines at mantle pressures and temperatures. *Contributions to Mineralogy and Petrology* **79**, 80–84.

Ryabchikov, I. D., Brey, G. P., Kogarko, L. N. & Bulatov, V. K. (1989). Partial melting of carbonated lherzolite at 50 kbar. *Geokhimiya* **N1**, 3–9.

Ryabchikov, I. D., Brey, G. P. & Bulatov, V. K. (1993). Carbonate melts coexisting with mantle peridotites at 50 kbar. *Petrology* **1**, 189–194.

Schneider, M. E. & Eggler, D. H. (1986). Fluids in equilibrium with peridotite minerals: implications for mantle metasomatism. *Geochimica et Cosmochimica Acta* **50**, 711–724.

Schrauder, M. & Navon, O. (1993). Solid carbon dioxide in a natural diamond. *Nature* **365**, 42–44.

Schrauder, M. & Navon, O. (1994). Hydrous carbonatitic mantle fluids in fibrous diamonds from Jwaneng, Botswana. *Geochimica et Cosmochimica Acta* **58**, 761–771.

Schrauder, M., Koeberl, C. & Navon, O. (1996). Trace element analysis of fluid bearing diamonds from Jwaneng, Botswana. *Geochimica et Cosmochimica Acta* **60**, 4711–4724.

Schreyer, W. (1999). Experimental aspects of UHP metamorphism: granitic systems. *International Geology Review* **41**, 701–710.

Shen, A. H. & Keppler, H. (1997). Direct observation of complete miscibility in the albite–H_2O system. *Nature* **385**, 710–712.

Stern, C. R. & Wyllie, P. J. (1981). Phase relationships of I-type granite with H_2O to 35 kb: the Dinkey Lakes biotite-granite from the Sierra Nevada batholith. *Journal of Geophysical Research* **86**, 10412–10422.

Sweeney, R. J. (1994). Carbonatite melt compositions in the Earth's mantle. *Earth and Planetary Science Letters* **128**, 259–270.

Takahashi, E. (1986). Melting of dry peridotite KLB-1 up to 14 GPa: implications on the origin of peridotitic upper mantle. *Journal of Geophysical Research* **91**, 9367–9382.

Taylor, W. R. & Green, D. H. (1988). Measurements of reduced peridotite–C–O–H solidus and implications for redox melting of the mantle. *Nature* **332**, 349–352.

Thibault, Y., Edgar, A. D. & Lloyd, F. E. (1992). Experimental investigation of melts from a carbonated phlogopite lherzolite: implications for metasomatism in the continental lithospheric mantle. *American Mineralogist* **77**, 784–794.

Thompson, A. B. (1992). Water in the Earth's upper mantle. *Nature* **358**, 295–302.

Wallace, M. E. & Green, D. H. (1988). An experimental determination of primary carbonatite magma composition. *Nature* **335**, 343–346.

Watson, S. & McKenzie, D. (1991). Melt generation by plumes: a study of Hawaiian volcanism. *Journal of Petrology* **32**, 501–537.

White, B. S. & Wyllie, P. J. (1992). Phase relations in synthetic lherzolite–H_2O–CO_2 from 20–30 kb, with applications to melting and metasomatism. *Journal of Volcanology and Geothermal Research* **50**, 117–130.

White, R. S. & McKenzie, D. P. (1989). Magmatism at rift zones: the generation of volcanic continental margins and flood basalts. *Journal of Geophysical Research* **94**, 7685–7729.

Wood, B. J., Bryndzia, L. T. & Johnson, I. K. E. (1991). Mantle oxidation state and its relationship to tectonic environment and fluid speciation. *Science* **249**, 337–345.

Wyllie, P. J. (1978). Mantle fluid compositions buffered in peridotite–CO_2–H_2O by carbonates, amphibole, and phlogopite. *Journal of Geology* **86**, 687–713.

Wyllie, P. J. (1979). Magmas and volatile components. *American Mineralogist* **64**, 469–500.

Wyllie, P. J. (1980). The origin of kimberlites. *Journal of Geophysical Research* **85**, 6902–6910.

Wyllie, P. J. (1987*a*). Transfer of subcratonic carbon into kimberlites and rare earth carbonatites. In: Mysen, B. O. (ed.) *Magmatic Processes: Physicochemical Principles. Geochemical Society Special Publication* **1**, 107–119.

Wyllie, P. J. (1987*b*). Metasomatism and fluid generation in mantle xenoliths: experimental. In: Nixon, P. H. (ed.) *Mantle Xenoliths*. New York: Wiley, pp. 609–621.

Wyllie, P. J. (1988). Solidus curves, mantle plumes, and magma generation beneath Hawaii. *Journal of Geophysical Research* **93**, 4171–4181.

Wyllie, P. J. (1995). Experimental petrology of upper mantle materials, processes and products. *Journal of Geodynamics* **20**, 429–468.

Wyllie, P. J. & Lee, W.-J. (1998). Model system controls on conditions for formation of magnesiocarbonatite and calciocarbonatite magmas from the mantle. *Journal of Petrology* **39**, 1885–1893.

Wyllie, P. J. & Ryabchikov, I. D., 1992. The distribution and behavior of volatile components in the Earth's mantle. *29th International Geological Congress, Kyoto, Japan. Abstract Volume 2*. Vienna: Graz University of Technology, p. 537.

Wyllie, P. J. & Tuttle, O. F., 1960. Experimental investigation of silicate systems containing two volatile components, Part 1. Geometrical considerations. *American Journal of Science* **258**, 498–517.

Zhang, Y. & Zindler, A. (1993). Distribution and evolution of carbon and nitrogen in Earth. *Earth and Planetary Science Letters* **117**, 331–345.